Research Article – Vol. 02, Issue 03, No. 10

Advanced in Engineering and Intelligence Systems

Journal Web Page: https://aeis.bilijipub.com

Multi-objective optimization of Energy, exergy, and exergo economic analyses a double-pressure flash-binary geothermal power system using zeotropic working fluid

Arivalagan Pugazhendhi [1,*] , Van Vang [2]

[1] *Faculty of Environment and Labour Safety, Ton Duc Thang University, Ho Chi Minh City, Viet Nam*
[2] *Ho Chi Minh City University of Transport, Ho Chi Minh City, Viet Nam*

Highlights

- Considering optimal placement and sizing of distributed generations in power market-based systems with using optimal power flow
- Considering local margin price as a factor of power market factor besides customer payment factor
- Applying the fast optimization method to find the optimal place and size of distributed generations
- Considering operation and economic factors in the optimal model to achieve the best point
- Analysis of both operation and economic factors after placement to illustrate the method's robustness.

Article Info

Received: 20 May 2023
Received in revised: 14 June 2023
Accepted: 11 July 2023
Available online: 30 September 2023

Keywords

Double-flash geothermal system,
Zeotropic mixture,
Energy and exergy analysis,
Multi-objective optimization,
Exergoeconomic

Abstract

Global warming due to greenhouse emission is the most annoying problem for sustaining life on earth. This paper combines a geothermal system with an organic Rankine cycle (ORC). Comprehensive thermodynamic and thermoeconomic analyses are employed to estimate the system performance and generate 3083 kW net power with 64.79% exergy efficiency and 3.51 years payback period. Parametric study is conducted to study the effect of some main parameters variation on the proposed system performance. Regarding the parametric study results, the vapor generator's evaporation temperature has the highest effect on the system exergy destruction. The second separator inlet pressure influences the net power production and exergy efficiency higher than other parameters. Then, the net present value is calculated for four geofluid and electricity costs. The electricity sale cots enhancement of about 33% increases the net profit by about 78.29%, and increasing the geofluid prices by about 38.4% declines the net profit of the proposed system by about 19.5%. Two multi-objective optimization scenarios are employed to optimize the energy efficiency with the payback period and exergy efficiency with the payback period. The optimization results indicate that the 20.63% energy efficiency with 3.58 years payback is the first scenario optimum point. The 65.53% exergy efficiency with 3.47 years payback period is the second scenario's optimum point.

Nomenclature

c	*Cost per unit of exergy* $[\$.GJ^{-1}]$	s	*Entropy* $kJ.kg^{-1}.K^{-1}$
CRF	*Capital Recovery Factor*	*ST*	*Steam Turbine*
Cond	*Condenser*	t	*Time* $[s]$
e	*Specific exergy* $[kJ.kg^{-1}]$	T	*Temperature* $[K]$
$\dot{E}$	*Exergy rate* $[kW]$	*VG*	*Vapor Generator*
EV	*Expansion Valve*	$\dot{W}$	*Power* $[kW]$
$\dot{E}x$	*Exergy flow* $[kW]$	Z	*Investment cost of components* $[\$]$
h	*Enthalpy* $[kJ.kg^{-1}]$	***Subscript and abbreviations***	

* Corresponding Author: Arivalagan Pugazhendhi
Email: arivalagan.pugazhendhi@tu.edu.vn

HST	*High Pressure Steam Turbine*	*cr*	*Critical*
K	*Interest rate [%]*	*D*	*Destruction*
LST	*Low Pressure Steam Turbine*	*Elec*	*Electrical*
$\dot{m}$	*Mass Flow Rate* $[kg.s^{-1}]$	*in*	*Inlet*
M M	*Molar Mass* $[g.mole^{-1}]$	*is*	*Isentropic*
Mix	*Mixer*	*PPT*	*Pinch Point Temperature [K]*
MOPSO	*Multi Objective Particle Swarm Optimization*	*sep*	*Separator*
NPV	*Net Present Value* [$]	*Tur*	*ORC Turbine*
O&M	*Operation and Maintenance*	*out*	*Outlet*
ORC	*Organic Rankine Cycle*	0	*Dead State*
P	*Pressure [kPa]*	1,2,3, …	*State Point*
PEC	*Purchased Equipment Cost [$]*	***Greek symbols***	
Pu	*Pump*	η	*Efficiency*
Q	*Heat* [*kJ*]	φ	*Maintenance Factor*

1. Introduction

Energy is one of the critical parameters for sustainable development in any nation. Technology progress and lifestyle change have led to increased energy demand, while the energy sources are limited, and checking the losses in the equipment is very important.[1]. Fossil fuels supply over 60-70% of power systems required energy to supply power demand [2], while their reservoirs are limited and cause global warming and CO_2 emission [3]. Nowadays governments have authorized restrict rules to decrease the fossil fuels environmental issues [4]. Besides, renewable energies have been introduced by energy researchers as the fossil fuels alternative [5]. But, renewable energy reservoirs such as wind, solar, and ocean waves are highly influenced by the climate condition except for the geothermal reservoir. Subsequently, the geothermal reservoir prepares a reliable and sustainable source to produce power [6]. The geothermal reservoirs are categorized based on their fluid temperature and physical state. At the temperature category assessment, the geothermal fluid with a temperature range of below 90 ˚C is considered as a low-temperature reservoir, between 90 to 150 ˚C is a moderate-temperature reservoir, and higher than 150 ˚C is a high-temperature reservoir. At the geofluid physical state category, the geothermal reservoirs are divided into dry-steam and moisture steam [7]. The primary geothermal systems were based on dry-steam, while this kind of geothermal resource is sacred and most of the probed geothermal reservoirs are moisture steam kind [8]. Hence, different arrangements of geothermal systems with the moisture steam working fluid have been studied.

2. Literature review

Yari [9] studied seven different binary configurations for a high-temperature geothermal system. Between seven considered configurations, the flash-binary configuration presented higher performance. Also, by adding an ORC subsystem with regenerative and internal heat exchanger, the highest energetic performance was obtained. Zeighami [10] probed proper working fluid for binary system which was run by different kinds of geothermal reservoirs. Regarded to his results, the refrigerant fluids are suitable for the low-temperature, and the hydrocarbon working fluids are proper for the moderate and high-temperature geothermal reservoirs. Mosaffa et al. [11] studied different binary systems that utilized geothermal resource as the inlet energy supplier from exergy and economic approach. They showed the best exergetic performance related to regenerative with internal heat exchanger ORC system, and the lowest total cost belongs to regenerative ORC. Pamudi et al. [11] proposed a single-flash and a double-flash geothermal power system for a geothermal reservoir in Dieng, Indonesia from energy viewpoint. They showed utilizing a double-flash system generates 6% more net power. Luo et al. [12] compared the exergetic performance of the binary and single-flash geothermal power system for different kinds of geothermal reservoirs in China. Their results indicated that for the geothermal reservoirs with less than 130 ˚C temperature, the binary system presents higher performance, and for the higher than 130 ˚C temperature, the single-flash system is suitable. Bina et al. [13] proposed a single and double-flash arrangements for Sabalan geothermal field and studied from exergetic and exergoeconomic approaches. Their results demonstrated double-flash system presents higher net output power and exergetic efficiency, while, single-flash system presents lower capital and operational cost. Then, in the other study, Bina et.al [14] applied different configuration of the ORC subsystem to the proposed double-flash system in the previous study. The energy and exergetic analysis of the new configuration illustrated that the ORC with internal heat exchanger includes higher performance and the ORC subsystem with a regenerative presents the best economic performance among considered configuration. Abdolalipouradl et al. [15] designed single-flash, double-flash, and triple-flash with an ORC subsystem for Sabalan, Iran geothermal field and compared them from exergetic and exergoeconomic viewpoint. They showed the double-flash system provides the highest net power and exegetic

efficiency and the single-flash system presents the lowest payback period. Guzovic et al. [16] compared employing a Kalina cycle and an ORC subsystems energetic performance for a geothermal power system in Croatia. Their results revealed that employing ORC subsystem presents 6% more net power than Kalina cycle.

Reviewing the previous studies demonstrates the ORC is the most employed subsystem for the geothermal power system. But, The ORC structure contains a constant evaporation process and this process provides considerable exergy destruction. In order to discount the exergy destruction, the zeotropic mixture utilization in the ORC subsystems can be useful [17]. These mixtures consist of different fluids with different physical properties. Hence, the evaporation process is performed at the variable temperature, and the exergy destruction and the temperature mismatch in the heat exchanger considerably decline [18]. Li et al. [19] proposed an ORC system with the pure and zeotropic working substance to compare their performance. Their obtained results indicated that the ORC system's performance with the zeotropic mixture presents considerably higher performance. Zhao et al. [20] experimentally compared an ORC system's performance with a pure substance and zeotropic mixture working substance and showed that the R245fa-R152a zeotropic mixture had a considerable higher thermal efficiency and net output power than R245fa as a pure working substance.

The previous studies demonstrate the flash-binary system was a hot-spotted configuration for the moderate-temperature geothermal power system. Also, applying the ORC system was a proper choice to recover the wasted energy of the geothermal power system, especially with zeotropic working fluid. Hence, this paper proposes a double flash-binary geothermal power system with an ORC subsystem to generate power. The first and second lows of thermodynamic and exergoeconomic analyses is conducted to obtain the designed system's energy, exergy and economic performances. Also, the following novelties are considered in this paper:

The zeotropic solution is selected as ORC subsystem to improve its performance.

Different zeotropic solutions are studied, and the Isopentane and Butene are selected as the ORC working fluids which are dry kind, and there is no need to be superheated.

Some design parameters variation's influence on the system operation's results is investigated as the parametric study.

Four different scenarios are considered to estimate the net present value of the proposed system.

Multi-objective optimizations are applied the proposed system via two optimization scenarios.

2.1.Paper structure

This paper contains different sections that demonstrate applied studies on the proposed system and are categorized as below contents:

Section. 2 demonstrates the system operation mode and streamlines that cross the components. In the section. 3, illustrates the employed assumption and input data to simulate the proposed system. Then, applied mass, energy, exergy, and exergoeconomic analysis are presented in Tables 3 and 4. The next section is the presentation of the results. This section contains different subsections. In the first subsection, the conducted simulation on the separator tank is validated by Wang et al. [21]. Then, parametric study results are shown in the section. 4. 2. The next subsection is the exergy destruction of the components which is illustrated via the Grassmann graph. Finally, the net present value calculation is presented for the four different scenarios of geofluid and electricity sale costs in the section 4.4. Section. 5 depict the performed multi-objective optimizations, in which two scenarios are followed to consider energy, exergy efficiencies and payback period. In the section. 6 the overall conclusions of this paper are presented.

3. System description

Fig. 1 illustrates the schematic diagram of the proposed system. The geo-fluid is extracted from underground (state. 1) and crosses the expansion valve (state. 2). The geo-fluid becomes two-phase in the expansion valve and enters to Sep unit (state. 2). During the flash process in the Sep unit, the vapor part is led to a steam turbine (state. 3) to expand and generate power. The liquid part after crossing the second expansion valve enters to the second Sep unit (state. 5). In the second Sep unit, the vapor part is extracted and leads to the low-pressure steam turbine. Besides, the liquid part enters the V.G.1 unit to provide the ORC subsystem required heat (state. 9). The high and low-pressure steam turbine outlet flows mixing process is performed in the Mix.1 unit and the mixed flow go to the Cond.1 unit. The V.G.1 outlet flow after crossing the third expansion valve is combined with Cond.1 outlet flow and brined to underground (state. 14). At the ORC subsystem, the zeotropic mixture's pressure increases via pump and reaches the sub-cooled liquid (state 18) then is led to the V.G.1 unit. In the V.G.1 unit, the zeotropic mixture becomes saturated vapor, enters the ORC turbine, and expands to generate power (state. 15). It is notable to mention that the utilized zeotropic mixture is

dry and does not require becoming superheated vapor. After expanding in the turbine, the zeotropic mixture enters Cond.2 (state 16) then is cooled down until it reaches saturated liquid at pump inlet pressure and completes the cycle.

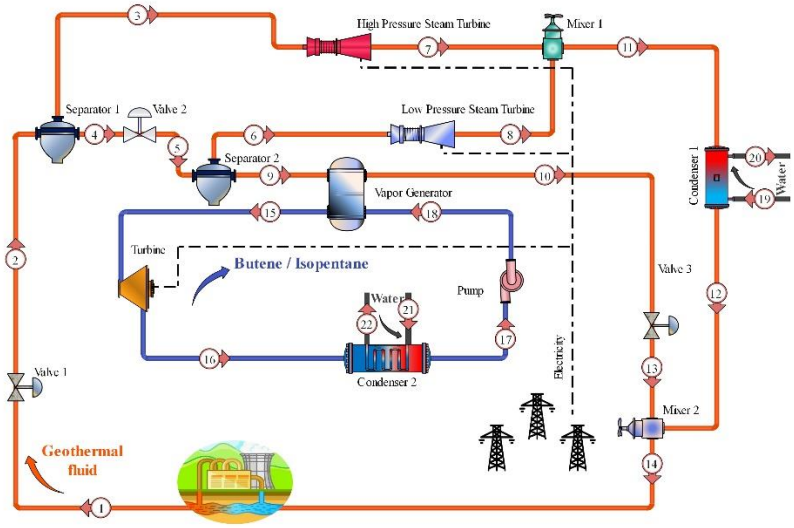

Fig. 2. The schematic diagram of the proposed system.

4. Mathematical modeling

In this section, the mass, energy, exergy and exergoeconomic equation that governed on all component are disused. The following assumptions are considered to simplify the proposed system simulation.

- All components operate under steady-state conditions [22].
- Change in kinetic and potential energies is negligible [22].
- The pressure drop in pipelines and heat exchangers is not considered [23].
- All components operation modes are assumed to be adiabatic [23].
- All turbines and pumps work at certain isentropic efficiencies [24].
- The throttling process in the expansion valve is assumed isenthalpic [24].
- Main properties of selected working fluids and main input parameters are presented in Table 1 and 2.

Table 1: The main characteristics of the fluids employed in this work.

Fluid	T_{cr} [K]	P_{cr} [kPa]	MM [$g.mol^{-1}$]	Type [$dT.ds^{-1}$]
Butene	419.29	4005.1	56.11	dry
Isopentane	460.35	3378	72.15	dry

Table 2: Some of the main input parameters and assumptions.

Parameter	symbol	Value	unit
Dead state temperature	T_0	293.15	[K]
Dead state pressure	P_0	101	[kPa]
Geothermal fluid mass flow rate	$\dot{m}_1$	45	[$kg.s^{-1}$]
Geothermal fluid enthalpy	h_1	1000	[$kJ.kg^{-1}$]
Geothermal fluid pressure	P_1	1200	[kPa]
Expansion valve 1 outlet pressure	P_2	1100	[kPa]
Expansion valve 2 outlet pressure	P_5	550	[kPa]
Steam turbine isentropic efficiency	$\eta_{is,ST}$	85	[%]
ORC turbine isentropic efficiency	$\eta_{is,Tur}$	85	[%]
ORC pump isentropic efficiency	$\eta_{is,Pump}$	85	[%]
Condenser pinch point temperature difference	$\Delta T_{PPT,Cond}$	10	[K]
Vapor generator pinch point temperature difference	$\Delta T_{PPT,VG}$	15	[K]

4.1.Mass and energy balance

This section presents the employed thermodynamic and thermoeconomic laws and equations. But, before presenting them, it is necessary to mention considered assumptions to simplify the simulation's process and use of thermodynamic and thermoeconomic principles as follows:

1. All devices operate at a steady-state [25].
2. All components are adiabatically designed [26].
3. The pressure drop in the heat transfer-based devices and pipelines is neglectable [27].
4. All pumps and turbines operate at the specific isentropic efficiency [28].

The expansion valves consist of the isenthalpic process [29].

4.2. Thermodynamic analysis

For thermodynamic analysis of the system, the method of the steady-state mass and energy balance formulas is followed by [30]:

$$\sum \dot{m}_{in} - \sum \dot{m}_{out} = 0 \quad (1)$$

$$\dot{Q}_{C.V} - \dot{W}_{C.V} = \sum (\dot{m}h)_{in} - \sum (\dot{m}h)_{out} \quad (2)$$

Where $\dot{m}$ denotes mass flow rate, $\dot{Q}$ indicates inlet and outlet heat transfer of control volume, $\dot{W}$ is work done by control volume boundary, h is enthalpy, *in* and *out* refers to inlet and outlet states.

Another important thermodynamic index is the exergy that is extracted from the thermodynimc's second low and presents the energy transfer's quality. In this way, the exergy balance for a control volume at the steady-state is expressed as [30]:

$$\dot{E}_Q - \dot{W} = \sum \dot{m}_{out} e_{out} - \sum \dot{m}_{in} e_{in} + \dot{E}_D \quad (3)$$

E and e denote the exergy and specific exergy, and subscripts of Q and D demonstrate the heat transfer and destructed exergy rate. The heat transfer exergy rate is calculated from [30]:

$$\dot{E}_Q = \sum \dot{Q}\left(1 - \frac{T_0}{T_b}\right) \quad (4)$$

Here, T_b depicts the boundary temperature that heat is transferred. T_0 refers the reference state temperature. The specific exergy is calculated as [30]:

$$e = h - h_0 - T_0(s - s_0) \quad (5)$$

where, s stands for the specific entropy. By considering the mentioned assumptions and presented thermodynamic analysis, the employed components' mass, energy, and exergy balances are demonstrated in Table 3.

Table 3: Mass, energy, and exergy balance equation for components.

Component	Mass balance	Energy balance	Exergy balance
Expansion valve 1	$\dot{m}_1 = \dot{m}_2$	$\dot{m}_1 h_1 = \dot{m}_2 h_2$	$\dot{E}_D^{EV,1} = \dot{E}_1 - \dot{E}_2$
Separator 1	$\dot{m}_2 = \dot{m}_3 + \dot{m}_4$	$\dot{m}_2 h_2 = \dot{m}_3 h_3 + \dot{m}_4 h_4$	$\dot{E}_D^{Sep,1} = \dot{E}_2 - (\dot{E}_3 + \dot{E}_4)$
Separator 2	$\dot{m}_5 = \dot{m}_6 + \dot{m}_9$	$\dot{m}_5 h_5 = \dot{m}_6 h_6 + \dot{m}_9 h_9$	$\dot{E}_D^{Sep,2} = \dot{E}_5 - (\dot{E}_6 + \dot{E}_9)$
Expansion valve 2	$\dot{m}_4 = \dot{m}_5$	$\dot{m}_4 h_4 = \dot{m}_5 h_5$	$\dot{E}_D^{EV,2} = \dot{E}_4 - \dot{E}_5$
High pressure steam turbine	$\dot{m}_3 = \dot{m}_7$	$\dot{W}_{HST} = \dot{m}_3 h_3 - \dot{m}_7 h_7 = (\dot{m}_3 h_3 - \dot{m}_7 h_{7s})\eta_{is,ST}$	$\dot{E}_D^{HST} = (\dot{E}_3 - \dot{E}_7) - \dot{W}_{HST}$
Low pressure steam turbine	$\dot{m}_6 = \dot{m}_8$	$\dot{W}_{LST} = \dot{m}_6 h_6 - \dot{m}_8 h_8 = (\dot{m}_6 h_6 - \dot{m}_8 h_{8s})\eta_{is,ST}$	$\dot{E}_D^{LST} = (\dot{E}_6 - \dot{E}_8) - \dot{W}_{LST}$
Condenser 1	$\dot{m}_{11} = \dot{m}_{12}, \dot{m}_{19} = \dot{m}_{20}$	$\dot{Q}_{Cond,1} = \dot{m}_{11} h_{11} - \dot{m}_{12} h_{12} = \dot{m}_{20} h_{20} - \dot{m}_{19} h_{19}$	$\dot{E}_D^{Cond,1} = (\dot{E}_{11} - \dot{E}_{12}) - (\dot{E}_{20} - \dot{E}_{19})$
Mixer 1	$\dot{m}_{11} = \dot{m}_7 + \dot{m}_8$	$\dot{m}_{11} h_{11} = \dot{m}_7 h_7 + \dot{m}_8 h_8$	$\dot{E}_D^{Mixer,1} = (\dot{E}_7 + \dot{E}_8) - \dot{E}_{11}$
Mixer 2	$\dot{m}_{14} = \dot{m}_{12} + \dot{m}_{13}$	$\dot{m}_{14} h_{14} = \dot{m}_{12} h_{12} + \dot{m}_{13} h_{13}$	$\dot{E}_D^{Mixer,1} = (\dot{E}_{12} + \dot{E}_{13}) - \dot{E}_{14}$
Expansion valve 3	$\dot{m}_{10} = \dot{m}_{13}$	$\dot{m}_{10} h_{10} = \dot{m}_{13} h_{13}$	$\dot{E}_D^{EV,2} = \dot{E}_{10} - \dot{E}_{13}$
Vapor generator	$\dot{m}_9 = \dot{m}_{10}, \dot{m}_{15} = \dot{m}_{18}$	$\dot{Q}_{VG} = \dot{m}_9 h_9 - \dot{m}_{10} h_{10} = \dot{m}_{15} h_{15} - \dot{m}_{18} h_{18}$	$\dot{E}_D^{VG} = (\dot{E}_9 - \dot{E}_{10}) - (\dot{E}_{15} - \dot{E}_{18})$
Turbine	$\dot{m}_{15} = \dot{m}_{16}$	$\dot{W}_{Tur} = \dot{m}_{15} h_{15} - \dot{m}_{16} h_{16} = (\dot{m}_{15} h_{15} - \dot{m}_{16} h_{16s})\eta_{is,Tur}$	$\dot{E}_D^{Tur} = (\dot{E}_{15} - \dot{E}_{16}) - \dot{W}_{Tur}$
Condenser 2	$\dot{m}_{16} = \dot{m}_{17}, \dot{m}_{21} = \dot{m}_{22}$	$\dot{Q}_{Cond,2} = \dot{m}_{16} h_{16} - \dot{m}_{17} h_{17} = \dot{m}_{22} h_{22} - \dot{m}_{21} h_{21}$	$\dot{E}_D^{Cond,2} = (\dot{E}_{16} - \dot{E}_{17}) - (\dot{E}_{22} - \dot{E}_{21})$
Pump	$\dot{m}_{17} = \dot{m}_{18}$	$\dot{W}_{Pump} = \dot{m}_{18} h_{18} - \dot{m}_{17} h_{17} = (\dot{m}_{18} h_{18s} - \dot{m}_{17} h_{17})/\eta_{is,Pump}$	$\dot{E}_D^{Pump} = \dot{W}_{Pump} - (\dot{E}_{18} - \dot{E}_{17})$

5. Exergoeconomic analysis

The power systems analyses based on the first and second law of thermodynamic show the energy and exergy performance assessments. These approaches do not satisfy the system's performance in all aspects. Applying the thermoeconomic analysis can be helpful to cover this gap. Hence, the economic relations are applied to the system's exergy balances to illustrate the exergoeconomic performance. The first economic equation is the cost

balance, which is applied to the employed components and demonstrated as [31]:

$$\dot{C}_{q,k} + \sum \dot{C}_{in,k} + \dot{Z}_k = \dot{C}_{w,k} + \sum \dot{C}_{out,k} \quad (6)$$

Where;

$$\dot{C} = c\dot{E}x \quad (7)$$

Also, the input and output exergies ($\dot{E}x_{in}$,$\dot{E}x_{out}$) are defined as the power ($\dot{E}x_w$) and heat transfer ($\dot{E}x_q$), and their unit costs are calculated as [31]:

$$\dot{C}_{in} = c_{in}\dot{E}x_{in} = c_{in}(\dot{m}_{in}ex_{in}) \quad (8)$$

$$\dot{C}_{out} = c_{out}\dot{E}x_{out} = c_{out}(\dot{m}_{out}ex_{out}) \quad (9)$$

$$\dot{C}_w = c_w\dot{E}x_w = c_w(\dot{m}_w ex_w) \quad (10)$$

$$\dot{C}_q = c_w\dot{E}x_q = c_q(\dot{m}_q ex_q) \quad (11)$$

In the above equations, $\dot{C}$ and c depict the cost rate and unit exergy cost, respectively.

The exergy destruction cost rate in the components is defined as [31]:

$$\dot{C}_{D,k} = c_{P,k}\dot{E}x_{D,k} \quad (12)$$

The component k's total cost is consisting of the capital cost (and the operation and maintenance (cost summation [31]:

$$\dot{Z}_k = \dot{Z}^{CI} + \dot{Z}^{OM} \quad (13)$$

In which, $\dot{Z}^{CI}$ is the capital cost and $\dot{Z}^{OM}$ denotes the operation and maintancne cost. Another economic analysis criteria is the annual investment cost and is calculated based on the component's total cost and estimated from the following [31]:

$$Z_k = \frac{CRF \times \varphi}{N \times 3600} \times \dot{Z}_k \quad (14)$$

Which Z_k depicts the purchasing cost of the component, N refers to the annual operating time and is assumed 3960 hours, φ defines the maintenance factor and is considered to be 1.06, and CRF is the capital recovery factor, which is obtained from the following equation [31]:

$$CRF = \frac{i(1+i)^n}{(1+i)^n - 1} \quad (15)$$

Where, i stands for the interest rate and is equal to 0.15. n demonstrates the components designed lifetime and is considered 20 years.

Also, the products' total cost rate is illustrated as the products cost summation and calculated as [31]:

$$\dot{c}_{tot} = \Sigma \dot{c}_p \quad (16)$$

The cost's data belong to the reference date, and to express the proposed system economic performance these data should be updated for the designed year. This update is conducted via chemical cost index, which its value for the 2020 date is about 668. In this way, the updated cost are estimated as [31]:

$$\text{Cost in target year} = \text{cost in reference year} \times \frac{\text{Cost index of target year}}{\text{Cost index of reference year}} \quad (17)$$

The net present value (NPV) is another economic analysis index that converts the next years cost to the present time through the interest rate. Also, this index illustrates the system's profitably and includes the payback period estimation. Hence, the NPV calculation helps the designers and investors draw the system's economic aspect roadmap. The NPV index is obtained from [31]:

$$NPV_n = -(FC) + \sum_{n=0}^{n} Y(1+i)^{-n} \quad (18)$$

FC stands for the fixed cost and is the components purchase costs' summation, and Y is the net cash flow [31]:

$$Y = AI - \left(C^{O\&M} + C_f\right) \quad (19)$$

The C_f depicts the fuel cost and in the current study is zero; because the proposed system fuel is supplied by the sun. Also, AI is the annual income and is estimated as [31]:

$$AI = \mathrm{AI} = \mathrm{c_{elec}} \times \mathrm{t_{year}} \times \dot{W}_{net} + \mathrm{c_{cool}} \times \mathrm{t_{year}} \times \dot{Q}_{cool} \quad (20)$$

$$C^{O\&M} = 0.06 \times FC \quad (21)$$

$$C_f = 0 \quad (22)$$

As mentioned, the NPV estimation leads to obtaining the system's payback period, which is defined as [31]:

$$PP = min\{n: NPV(n) > 0\} \quad (23)$$

The exergoeconomic analysis for the proposed system's components is demonstrated in Table 2:

Table 4: Cost function, cost balance and auxiliary equations for components

Components	Cost functions	Cost balance	Auxiliary equations
Expansion valve 1	$\mathrm{PEC}_{\mathrm{EV},1} = 114.5 \times \dot{m}_1$	$\dot{C}_1 + \dot{Z}_{\mathrm{EV},1} = \dot{C}_2$	–
Separator 1	$\mathrm{PEC}_{\mathrm{Sep},1} = 0$	$\dot{C}_2 + \dot{Z}_{\mathrm{Sep},1} = \dot{C}_3 + \dot{C}_4$	$c_4 = c_3$
Separator 2	$\mathrm{PEC}_{\mathrm{Sep},2} = 0$	$\dot{C}_5 + \dot{Z}_{\mathrm{Sep},2} = \dot{C}_6 + \dot{C}_9$	$c_6 = c_9$
Expansion valve 2	$\mathrm{PEC}_{\mathrm{EV},2} = 114.5 \times \dot{m}_4$	$\dot{C}_4 + \dot{Z}_{\mathrm{EV},2} = \dot{C}_5$	–
High pressure steam turbine	$\mathrm{PEC}_{\mathrm{HST}} = 3880.5 \times \dot{W}_{\mathrm{HST}}^{0.7} \left(1 + \left(\frac{0.05}{0.92 - \eta_{\mathrm{is,ST}}}\right)^3\right)\left(1 + 5 \times 2.71^{\frac{(T_3 - 866)}{10.42}}\right)$	$\dot{C}_3 + \dot{Z}_{\mathrm{HST}} = \dot{C}_7 + \dot{C}_{\mathrm{W,HST}}$	$c_3 = c_7$
Low pressure steam turbine	$\mathrm{PEC}_{\mathrm{LST}} = 3880.5 \times \dot{W}_{\mathrm{LST}}^{0.7} \left(1 + \left(\frac{0.05}{0.92 - \eta_{\mathrm{is,ST}}}\right)^3\right)\left(1 + 5 \times 2.71^{\frac{(T_6 - 866)}{10.42}}\right)$	$\dot{C}_6 + \dot{Z}_{\mathrm{LST}} = \dot{C}_8 + \dot{C}_{\mathrm{W,LST}}$	$c_6 = c_8$
Condenser 1	$\mathrm{PEC}_{\mathrm{Cond\ 1}} = 8000\left(\frac{A_{\mathrm{Cond},1}}{100}\right)^{0.6}$	$\dot{C}_{11} + \dot{C}_{19} + \dot{Z}_{\mathrm{Cond},1} = \dot{C}_{12} + \dot{C}_{20}$	$c_{19} = 0, c_{11} = c_{12}$
Mixer 1	$\mathrm{PEC}_{\mathrm{Mixer},1} = 0$	$\dot{C}_7 + \dot{C}_8 + \dot{Z}_{Mixer,1} = \dot{C}_{11}$	–
Mixer 2	$\mathrm{PEC}_{\mathrm{Mixer},2} = 0$	$\dot{C}_{12} + \dot{C}_{13} + \dot{Z}_{Mixer,2} = \dot{C}_{14}$	–
Expansion valve 3	$\mathrm{PEC}_{\mathrm{EV},3} = 114.5 \times \dot{m}_{10}$	$\dot{C}_{10} + \dot{Z}_{\mathrm{EV},3} = \dot{C}_{13}$	–
Vapor generator	$\mathrm{PEC}_{\mathrm{VG}} = 17500\left(\frac{A_{\mathrm{VG}}}{100}\right)^{0.6}$	$\dot{C}_9 + \dot{C}_{18} + \dot{Z}_{\mathrm{VG}} = \dot{C}_{10} + \dot{C}_{15}$	$c_9 = c_{10}$
Turbine	$\mathrm{PEC}_{\mathrm{Tur}} = 4750\left(\dot{W}_{\mathrm{Tur}}\right)^{0.75}$	$\dot{C}_{15} + \dot{Z}_{\mathrm{Tur}} = \dot{C}_{16} + \dot{C}_{\mathrm{W,Tur}}$	$c_{15} = c_{16}$
Condenser 2	$\mathrm{PEC}_{\mathrm{Cond\ 2}} = 8000\left(\frac{A_{\mathrm{Cond},2}}{100}\right)^{0.6}$	$\dot{C}_{16} + \dot{C}_{21} + \dot{Z}_{\mathrm{Cond},2} = \dot{C}_{17} + \dot{C}_{22}$	$c_{21} = 0, c_{16} = c_{17}$
Pump	$\mathrm{PEC}_{\mathrm{Pump}} = 200\left(\dot{W}_{\mathrm{Pump}}\right)^{0.65}$	$\dot{C}_{17} + \dot{Z}_{\mathrm{Pump}} + \dot{C}_{\mathrm{W,Pump}} = \dot{C}_{18}$	–

5.1. Performance criteria

In this section, the performance criteria of proposed cases of study have been studied.

The net power production at ORC subsystem and whole system are calculated as:

$$\dot{W}_{\mathrm{ORC}} = \dot{W}_{\mathrm{Tur}} - \dot{W}_{\mathrm{Pump}} \quad (26)$$

$$\dot{W}_{\mathrm{tot}} = (\dot{W}_{\mathrm{HST}} + \dot{W}_{\mathrm{LST}} + \dot{W}_{\mathrm{Tur}}) - \dot{W}_{\mathrm{Pump}} \quad (27)$$

Also, the energy and exergetic efficiency of ORC subsystem and whole system estimated from following equations:

$$\eta_{\mathrm{energy,ORC}} = \frac{\dot{W}_{\mathrm{ORC}}}{\dot{m}_9 \times (h_9 - h_{10})} \quad (28)$$

$$\eta_{\mathrm{energy,tot}} = \frac{\dot{W}_{\mathrm{tot}}}{\dot{m}_1 \times (h_1 - h_{14})} \quad (29)$$

$$\eta_{\mathrm{exergy,ORC}} = \frac{\dot{W}_{\mathrm{ORC}}}{\dot{E}_9 - \dot{E}_{10}} \quad (30)$$

$$\eta_{\mathrm{exergy,tot}} = \frac{\dot{W}_{\mathrm{tot}}}{\dot{E}_1 - \dot{E}_{14}} \quad (31)$$

6. Results and discussion

6.1. Validation of the conducted simulation

The mass, energy, exergy, and exergoeconomic analysis are applied to all study cases via ESS code. Before presenting the obtained results, the flash separator tank simulation's validation is made by flash process's pressure variation versus power production rate and the obtained results are compared with Wang et al. [21]. Fig. 2 presents the comparison results and its data indicate simulation accuracy and low divergence.

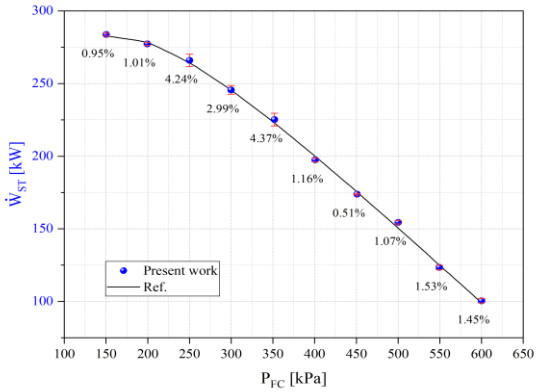

Fig. 2. The validation of flash cycle simulation with Wang et al. [21].

6.2. Parametric study

In this section, the design parameters variation's influences on the system operation indexes are demonstrated . The conducted parametric study contains two parts of ORC subsystem parameters and geothermal system parameters. The first part presents the effect of zeotropic mixture mass fraction and vapor generator's evaporation temperature on the total and ORC subsystem exergy destruction, net output power, energy efficiency, exergy efficiency, and payback period. The second part shows the effect of separators inlet pressure on the ORC subsystem, low-pressure steam turbine, high-pressure steam turbine, and total net power production, total energy and exergy efficiencies, total exergy destruction, and payback period.

6.2.1 The ORC subsystem parameters effect

6.2.1.1 The net output power

Fig. 3a presents the effect of zeotropic mixture mass fraction and vapor generator's evaporation temperature variation on the ORC subsystem net power production. Assuming the constant evaporation temperature, the Butene mass fraction augment in the mixture improves the ORC subsystem net output power then declines it. Also, the maximum net power production for the higher evaporation temperature is presented at the high mass fractions. Increasing the evaporation temperature at the constant mass fraction raises the ORC subsystem net power and decreases it. The optimum point is performed at a higher mass fraction for the higher evaporation temperature. The overall results indicate that the maximum net power production of the ORC subsystem is presented by the mass fraction of 0.4 and 362 K evaporation temperature. The total net power follows the ORC subsystem trend, which is shown in Fig. 3b. But, the maximum net power production is presented by the mass fraction of 0.5 and 363 K evaporation temperature.

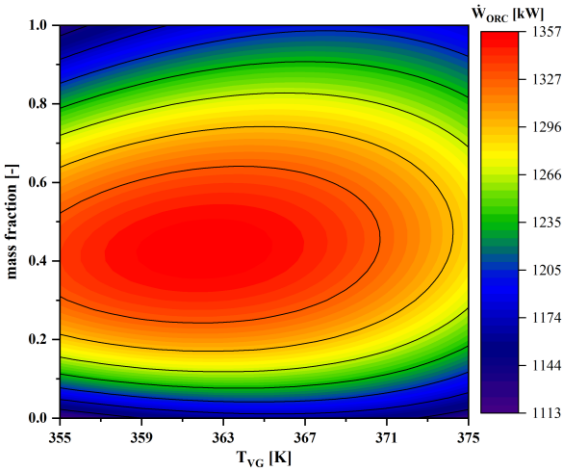

Fig. 3. a. Effect of mass fraction and vapor generator's evaporation temperature on the ORC subsystem net power production.

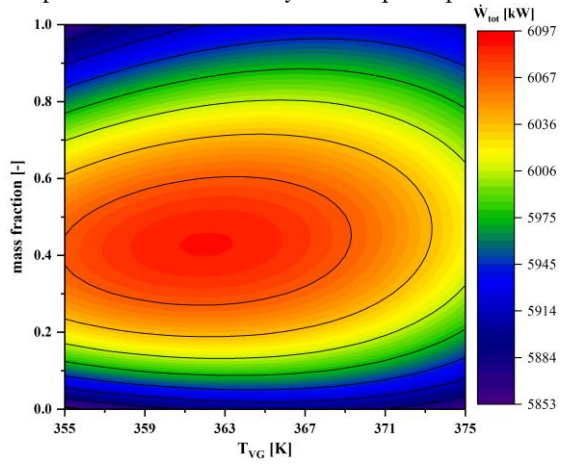

Fig. 3. b. Effect of mass fraction and vapor generator's evaporation temperature on the total net power production.

6.2.1.2 Exergy destruction

Figs. 4a and b show the ORC and total exergy destruction behavior by change in the vapor generator's temperature and mass fraction of the ORC system's working fluid, respectively. Increasing the evaporation decreases the temperature miss-match in the vapor generator and leads to declining the exergy destruction in the mentioned unit. Subsequently, the exergy destruction in the ORC subsystem and whole system decreases at the all mass fraction dominance. But, the mass fraction variation influences the exergy destruction with the complex trend. Increasing Butene mass portion in the working mixture decreases the exergy destruction in the ORC subsystem until the mass fraction of 0.4 and for the higher portion, enhances it. This trend is performed for all considered evaporation temperatures in the vapor generator. This trend is also performed for the total exergy destruction with the same mass fraction. So that, the minimum exergy destruction for the ORC subsystem and proposed system is presented by the mass fraction of 0.4 and 375 K evaporation temperature.

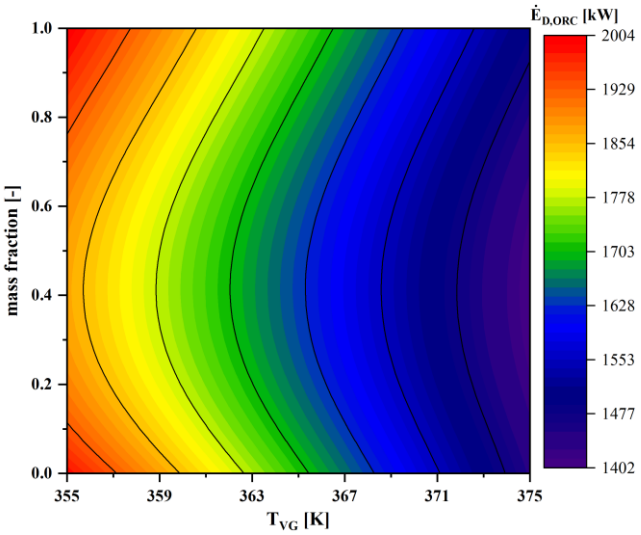

Fig. 4. a. Effect of mass fraction and vapor generator's evaporation temperature on the ORC subsystem exergy destruction.

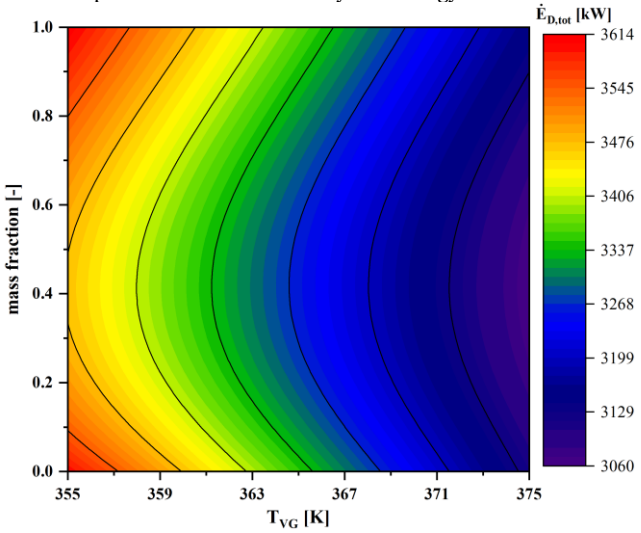

Fig. 4. b. Effect of mass fraction and vapor generator's evaporation temperature on the total exergy destruction of the proposed system.

6.2.1.3 Energy efficiency

Increasing the butene mass fraction in the zeotropic mixture improves the energy efficiency up to the mass fraction of 0.4; then, by increasing the mass fraction, the energy efficiency declines for the constant evaporation temperature and all evaporation temperature follows this trend. Besides, increasing the evaporation temperature at the constant mass fraction increases the energy efficiency. So, the maximum energy efficiency is presented by the mass fraction of 0.4 and 375 K evaporation temperature. As shown in Figs. 5a and b, which illustrate the effect of the zeotropic mixture mass fraction and evaporation temperature variation on the ORC subsystem and total energy efficiency. The energy efficiency trend is the same in the ORC subsystem and the whole system. Even the maximum energy efficiency is presented by the same at both systems. But, the zeotropic mass fraction variation influences the ORC subsystem energy efficiency higher than the total energy efficiency. So that, the trend of decreasing and increasing is performed with the higher slope.

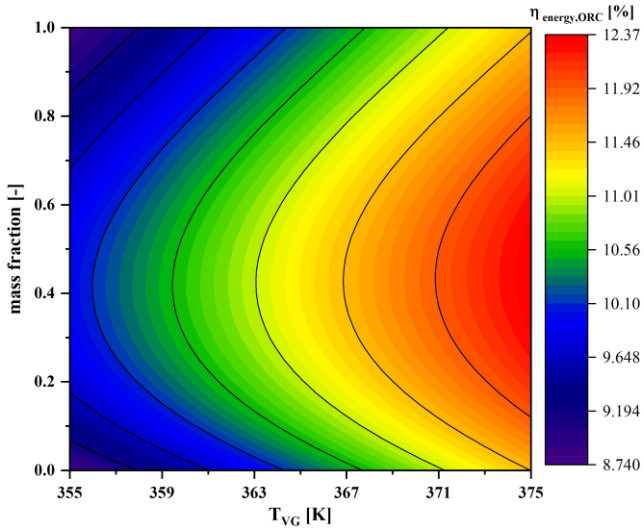

Fig. 5. a. Effect of mass fraction and vapor generator's evaporation temperature on the ORC subsystem energy efficiency.

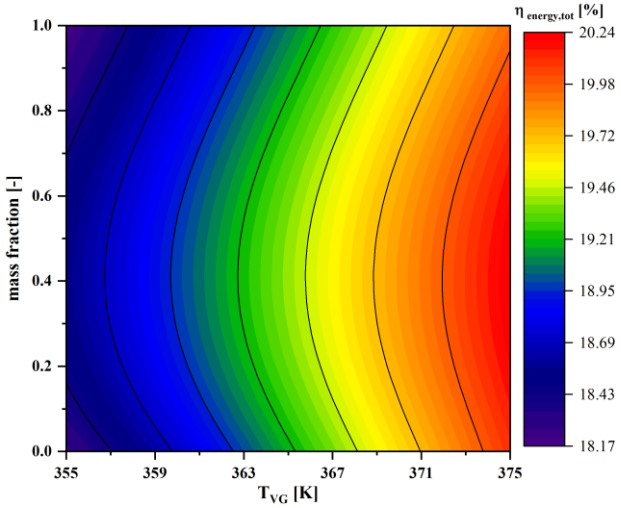

Fig. 5. b. Effect of mass fraction and vapor generator's evaporation temperature on the total energy efficiency of the proposed system.

6.2.1.4 Exergy efficiency

Figs. 6a and b show the effect of zeotropic mixture mass fraction and evaporation temperature in the vapor generator variation on the ORC subsystem and total exergy efficiency. As mentioned in the previous sections, increasing the Butene mass fraction first increases the net power and exergy destruction in the ORC subsystem and whole system for the constant evaporation temperature. So, the exergy efficiency increases up to the mass fraction of 0.4. Then, by increasing the mass fraction, the exergy efficiency decreases. On the other hand, increasing the evaporation temperature decreases the exergy destruction for the constant mass fraction, and the net output power first increases then declines. But, decreasing the exergy

destruction overcomes net output power at high evaporation temperature. Subsequently, the exergy efficiency of the ORC subsystem and whole system increases via increasing the evaporation temperature. Also, the overall results of the mass fraction and evaporation variation influence on the exergy reveal that the maximum exergy efficiency is presented by the mass fraction of 0.4 and 375 K evaporation temperature for the ORC subsystem and proposed system.

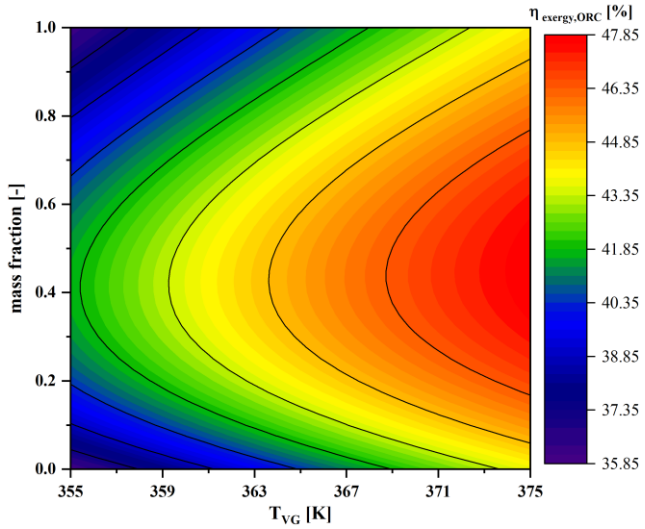

Fig. 6. a. Effect of mass fraction and vapor generator's evaporation temperature on the ORC subsystem exergy efficiency.

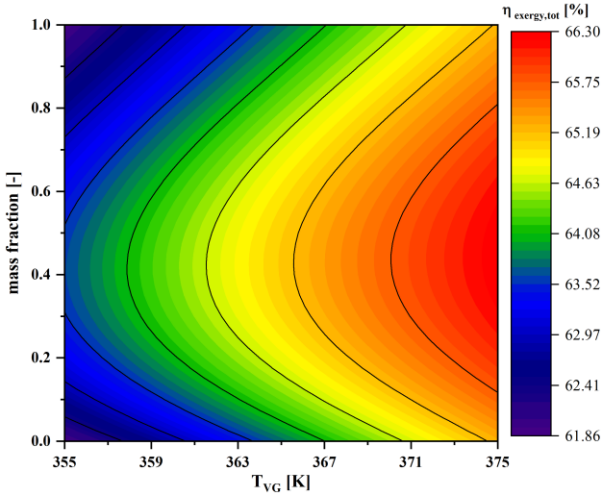

Fig. 6. b. Effect of mass fraction and vapor generator's evaporation temperature on the total exergy efficiency of the proposed system.

6.2.1.5 The payback period

Fig. 7 illustrates the effect of zeotropic mixture mass fraction and vapor generator's evaporation temperature on the proposed system payback period. As shown in Fig. 7, by assuming constant evaporation, the Butene mass portion's augment in the zeotropic mass fraction decreases the proposed system payback period but, for the higher mass portion of Butene the system's PP deals with an up-trend. It is notable to mention that the reversal point of the payback period trend is performed at the high-level mass portion of Butene by increasing the evaporation temperature in the vapor generator unit. Besides, at the constant mass fraction, increasing the evaporation temperature decreases the system's PP and enhances it. The pivot point of the payback period at the constant mass fraction is different at the various mass fractions. So that, up to the mass fraction of 0.4, the reversal point is performed at the lower evaporation temperature. For the mass fractions of higher than 0.4, the payback period trend's reversal point appears at the higher evaporation temperature. Also, the minimum payback period is presented by the mass fraction of 0.4 and 363 K evaporation temperature.

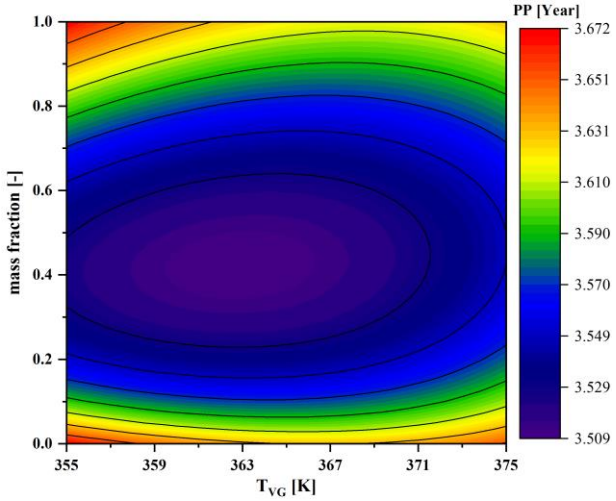

Fig. 7. The mass fraction and vapor generator's temperature variation's impact on the system's payback period.

6.2.2 The geothermal system's parameters effect

6.2.2.1 Effect of the first separator inlet pressure

Figs. 8a and b show the effect of the first separator inlet pressure on the main metric performance criteria of the proposed system. Increasing the first separator inlet pressure causes to perform the flashing process at higher pressure. So, fewer vapors are extracted from the separator and enter the HST unit. On the other hand, more liquid enters the second separator and leads to increasing the LST unit inlet vapor. Therefore, the HST unit power production and exergy destruction decline, and the LST unit generate more power. Besides, the ORC subsystem performance does not influence by the first separator inlet pressure, and the ORC subsystem net power production remains constant. The LST, HST, and ORC power production variation leads to increasing the total net power production. Also, decreasing the HST unit exergy destruction decreases the whole system's exergy destruction. The summation of total net power production

improvement and exergy destruction declines refers to increasing the energy and exergy efficiencies of the proposed system. Also, increasing the separator inlet pressure affects the capital, operation, and maintenance cost higher than the product purchased cost and increases the system's PP index.

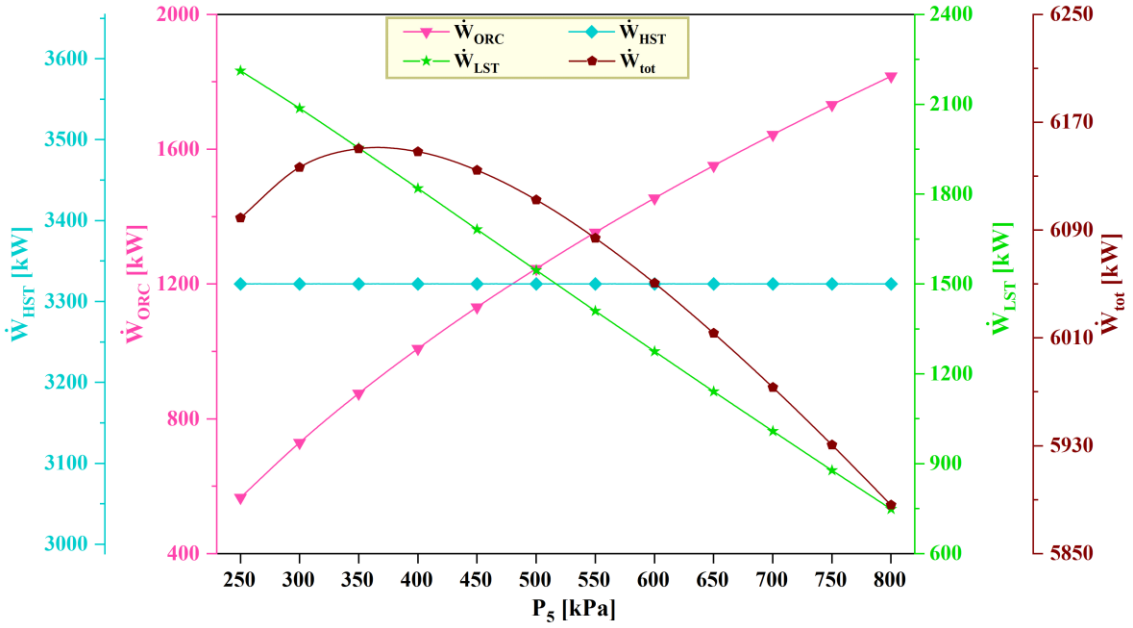

(a)

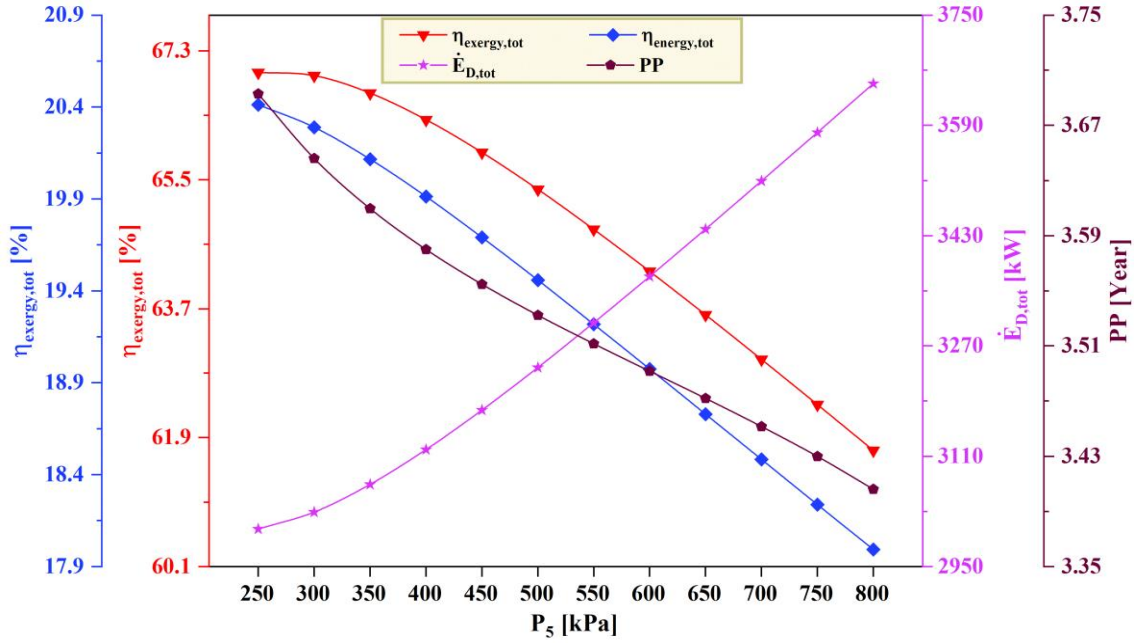

(b)

Fig. 8. Effect of first separator inlet pressure variation on the main metrics performance criteria of the proposed system.

6.2.2.2 Effect of the second separator inlet pressure

The second separator criteria variation does not influence the HST unit performance, and its power production remains constant. On the other hand, increasing the second separator inlet pressure reduces the LST unit inlet mass flow rate and subsequently declines the LST unit power generation. Besides, more mass flow rate enters the vapor generator unit. Increasing the V.G unit inlet mass flow rate increases the ORC subsystem inlet energy and exergy destruction in the V.G unit. Therefore, the ORC subsystem's net power production

rises. Since the V.G unit exergy destruction is considerable, increasing the V.G unit exergy destruction influences the total exergy destruction and increases it. Increasing the ORC net output power increases, the total power production but, for the higher pressure, the LST unit power generation drops overcomes the ORC power production rises and decreases the total net output power. The total net output power declines besides the total exergy destruction increasing leads to decreasing the energy and exergy efficiencies of the proposed system. Also, increasing the second separator inlet pressure decreases the payback period of the proposed system. More details of the second separator inlet pressure's effect on the proposed system performance are shown in Figs. 9a and b.

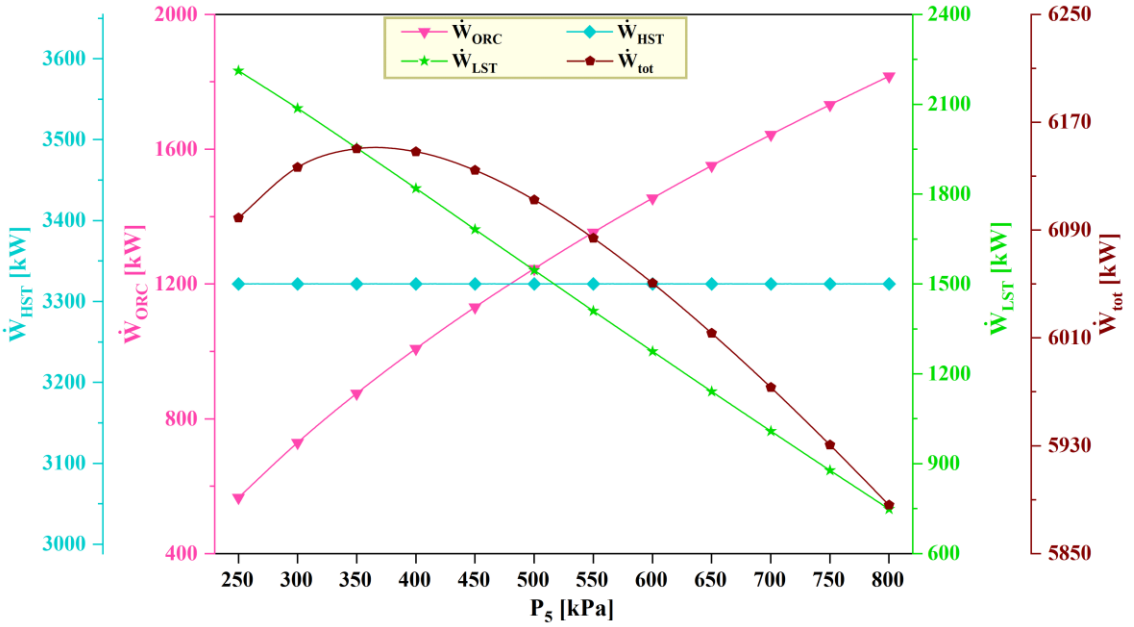

(a)

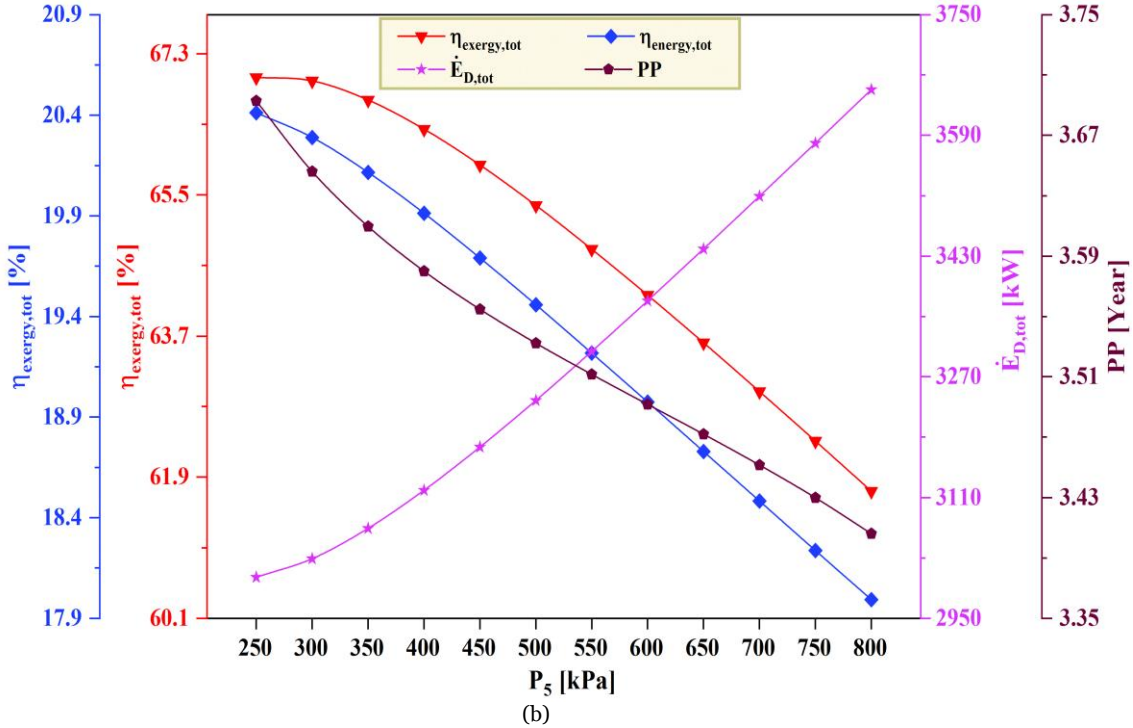

(b)

Fig. 9. Effect of second separator inlet pressure variation on the main metrics performance criteria of the proposed system.

6.3. The Grassmann diagram of the proposed system

Fig. 10 illustrates the exergy destruction distribution in the system components as the Grassmann diagram. The Grassmann diagram's information shows that the vapor generator contains the highest exergy destruction by about 903 kW. The HST unit with 564 kW exergy destruction is placed in the second rank. Since all employed components operate at the adiabatic condition, the mixer and separator units present zero exergy destruction. Also, the condenser units include considerable exergy destruction so that the geothermal condenser destroys 501 kW exergy flow. The overall results of the exergy destruction indicate the total exergy destruction in the proposed system obtains about 3083 kW. Also, the employed turbines contain 33.27%, and the utilized heat exchangers include 57.63% of the total exergy destruction. The rest of the components have the 9.1% portion in the proposed system's exergy destruction. Furthermore, the vapor generator presents 29.28% of the total exergy destruction alone.

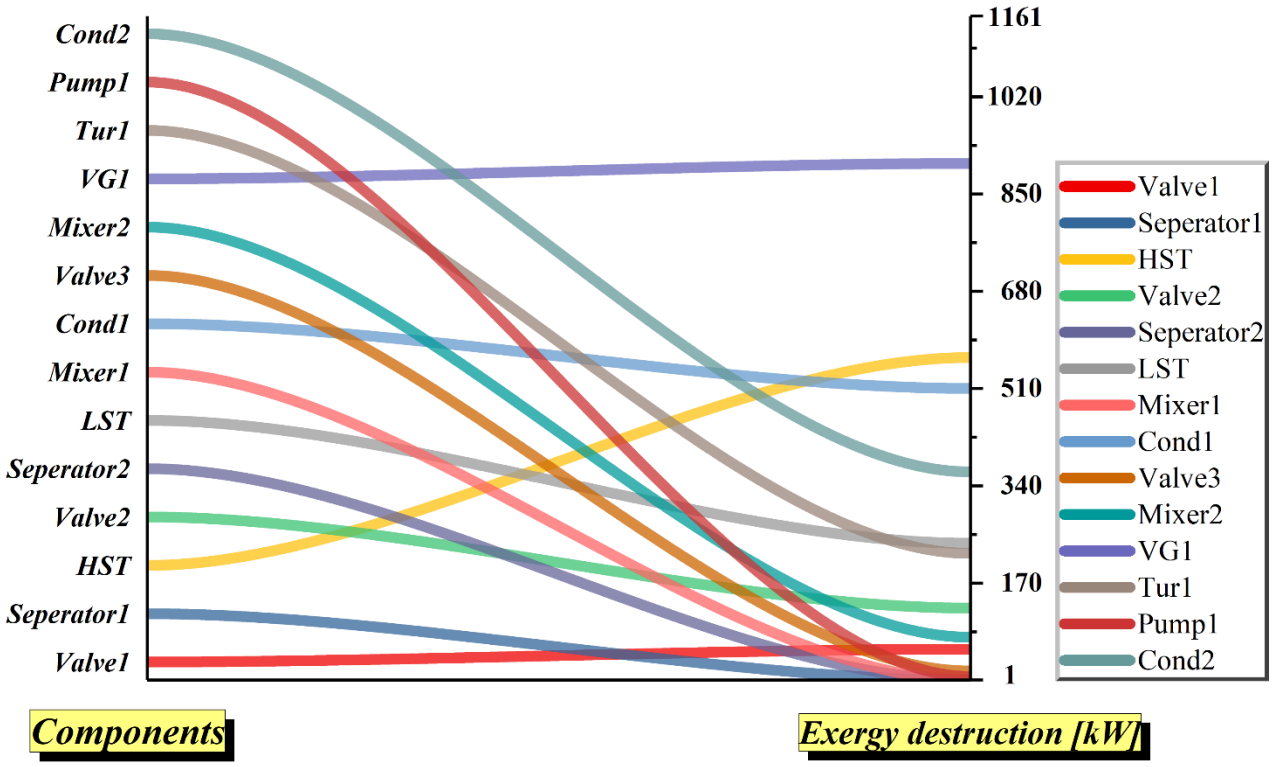

Fig. 10. The Grassmann diagram of the proposed system.

6.4. The NPV index evaluation

The net present value (NPV) estimation leads to evaluating the proposed system's payback period and profitably in the designed lifetime. Also, it shows the financial roadmap of the system's performance from economic approach. In this way, the NPV of the proposed system is estimated for four different geofluid and electric sale prices. Fig. 11 shows the NPV of the proposed system for the four different scenarios of geofluid and electricity sale prices. In the first scenario, the geofluid and electricity sale prices are considered 1.3 $/GJ and 0.09 $/kWh, respectively. At these prices, the proposed system's payback period is obtained by about 3.51 years, and the system presents the 10.13 M$ net profit. The geofluid and electricity sale prices are assumed in the second scenario are 1.8 $/GJ and 0.06 $/kWh, respectively. Considering these prices provides the payback period longer than the system's lifetime. Subsequently, at the 20 years' system lifetime, the proposed system does not present any profit and provides 1.41 M$ lost. In the third scenario, the geofluid price is considered 1.3 $GJ, and the electricity sale price is assumed 0.12 $/kWh. At this sale and incoming prices scenario, the payback period is obtained about 2.53 years with 18.13 M$ net profit during the 20 years of the system lifetime. The geofluid and electricity sale prices in the fourth scenario are considered 1.8 $/GJ and 0.12 $/kWh, respectively. At these prices, the proposed system's payback period is obtained by about 2.84 years, and the

system presents the 14.58 M$ net profit. Comparing the first and third scenarios results show that increasing the electricity sale prices by about 33% decreases the payback period by about 29%, and 78.9% improves the net profit. Also, in the fourth scenario, the electricity sale price is the same as scenario third, but the geofluid price increases about 38.4%. This increment in the geofluid price increases the payback period by about 12.4% and declines the proposed system's net profit by about 19.5%.

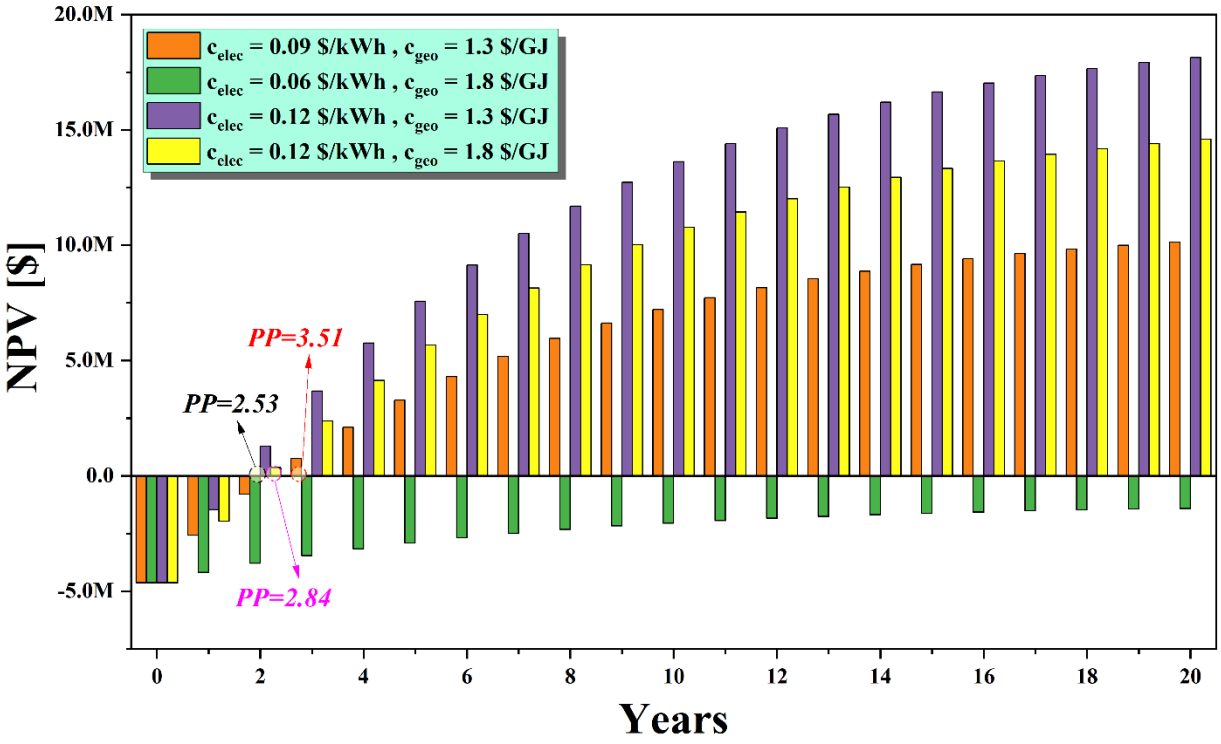

Fig. 11. The NPV evaluation for different price scenarios.

7. Optimization

Comprehensive energy, exergy, and exergoeconomic analysis have been performed to evaluate the proposed system performance. The proposed system presents 6083 kW net power with 64.79% exergy and 19.22% energy efficiencies, and by considering the 1.3 $/GJ geofluid price and 0.09 $/kWh electricity sale price, the payback period is obtained about 3.51 years at the base condition of system operation. Hence, an MOPSO approach is conducted to obtain the optimum condition of system operation mode. The first and second separator's inlet pressure, zeotropic working fluid's mass fraction, and vapor generator's evaporation temperature are considered as the decision-maker parameters. Two optimization scenarios are employed to obtain the optimum operating condition of the proposed system. The first scenario optimizes the energy efficiency and payback period. Employing the MOPSO approach to optimize the design system performs a Pareto-frontier, and the scatter distribution of the optimization parameters is shown in Fig. 12. Then, an LINMAP method is utilized to select the best optimum point in the Pareto-frontier, in which the 20.63% and 3.58 years' energy efficiency and payback period, respectively, are chosen as the optimum point. More details of the Pareto-frontier and LINMAP code results are presented in Fig. 13. The second optimization scenario considers the cost function of the exergy efficiency and payback period. Subsequently, the scatter distribution of the optimization variables to perform a Pareto-frontier is shown in Figure 14. Then, the LINMAP method application chooses the 53.57% exergy efficiency and 3.47 years' payback period as the final optimum operation mode, which is plotted in the Figure 15 in detail. Furthermore, the net present value of the proposed system is estimated for the considered prices of the previous section at the optimum condition. Applying optimization leads to economic performance enhancement. Hence, for the geofluid price of 1.3 $/GJ and 0.09$/kWh electricity

sale price the payback period is obtained by about 3.47 years. Considering the geofluid and electricity sale prices of 1.8 $/GJ and 0.06 $/kWh, respectively, even after applying the optimization the payback period is estimated about longer than system lifetime. For the geofluid price of 1.3 $/GJ and electricity sale price of 0.12 $/kWh the payback period at the optimum condition is obtained by about 2.51 years, and for the geofluid and electricity sale prices of 1.8 $/GJ and 0.12 $/kWh, respectively, the proposed system payback period is evaluated by about 2.81 years. The NPV comparison of the different prices at the optimum condition demonstrates that the applying optimization to the first prices scenario improves the NPV higher than the other prices scenarios. Also, the comparison of the proposed system's NPV for the considered prices at the optimum sate is shown in Fig. 16 with more details.

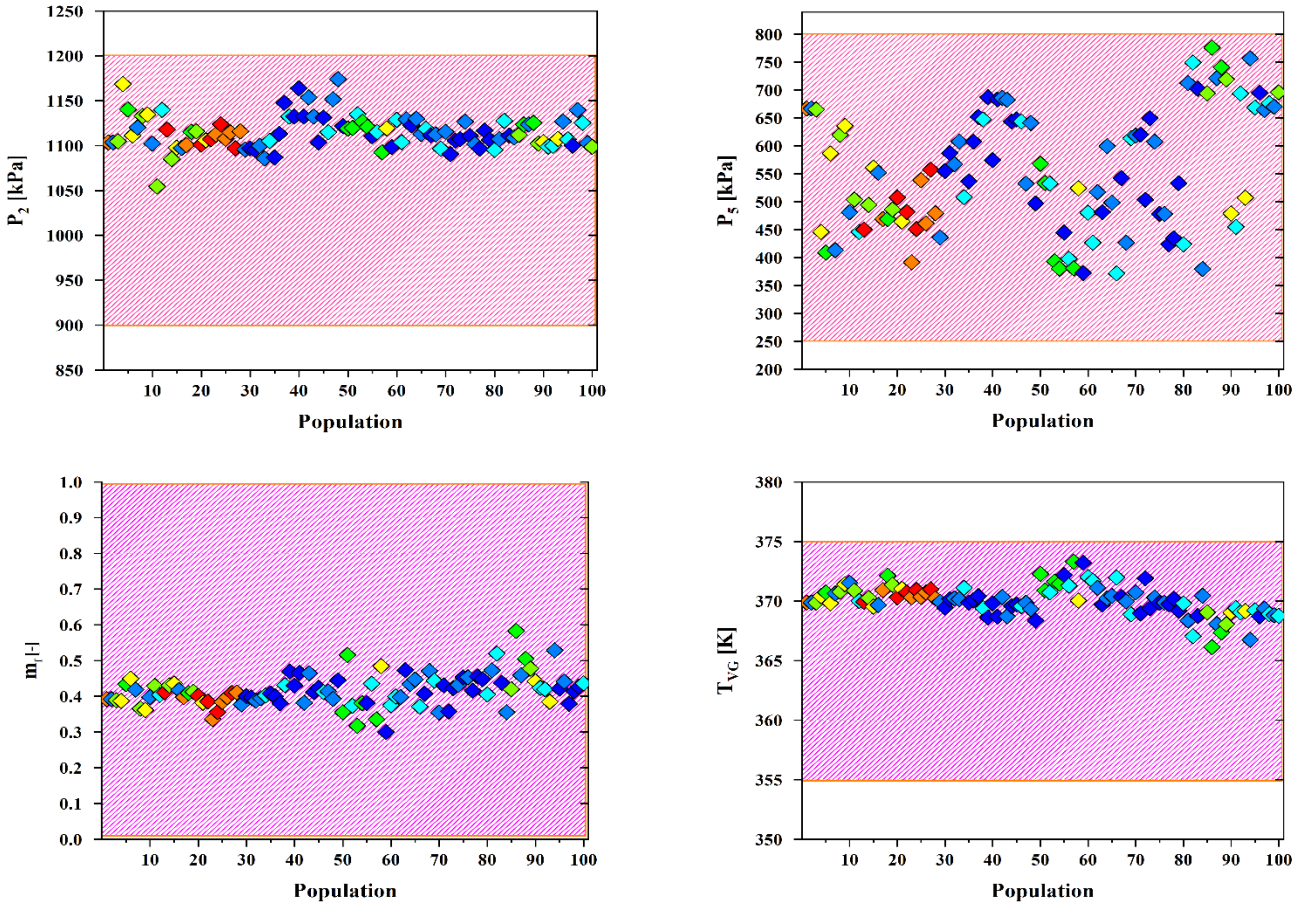

Fig. 12. The scatter distribution of the optimization parameters of the first optimization scenario.

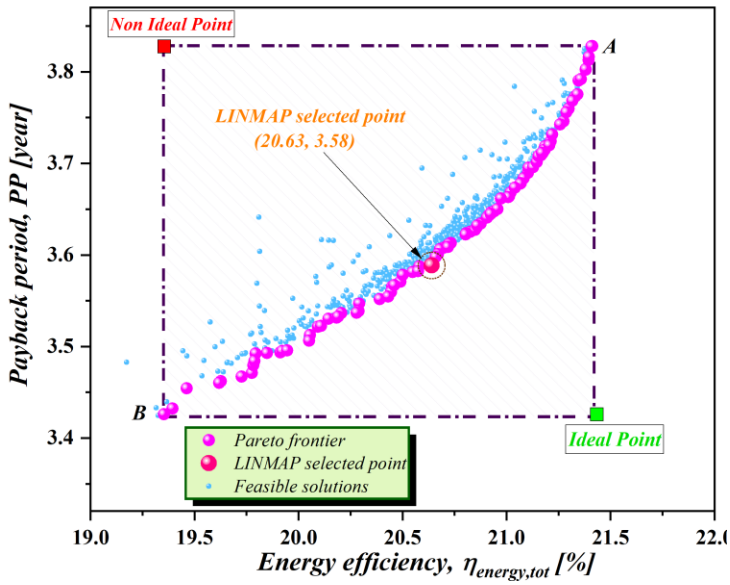

Fig. 13. The optimization result of the first optimization scenario.

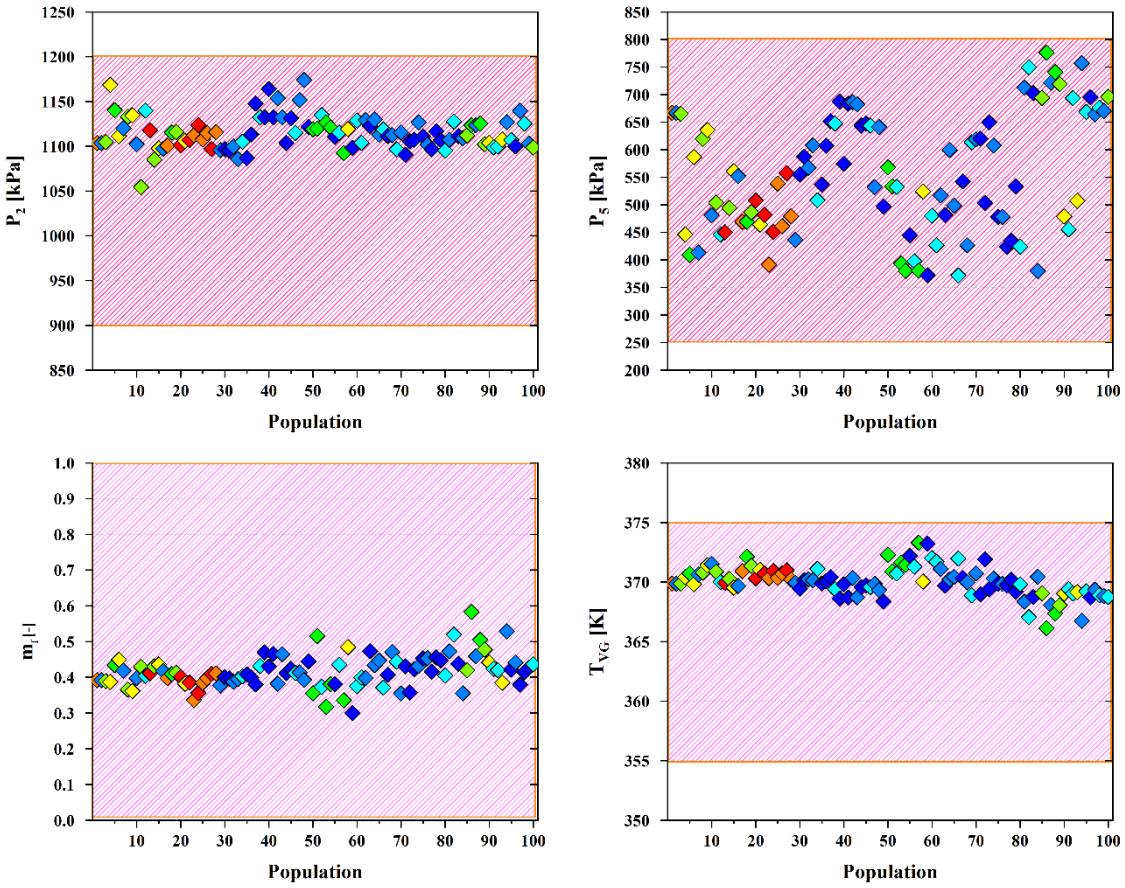

Fig. 14. The scatter distribution of the optimization parameters the second optimization scenario.

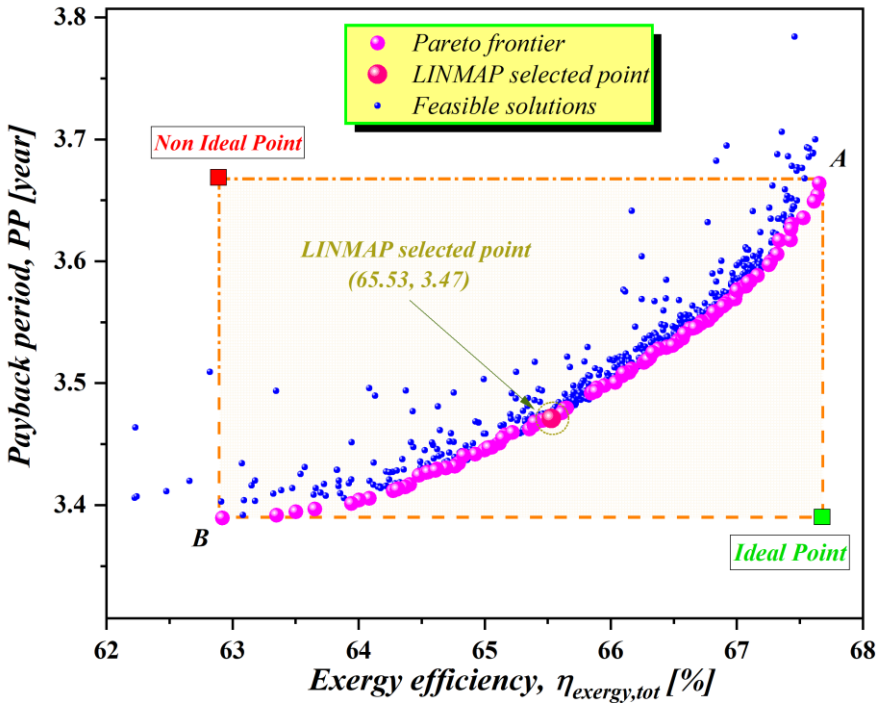

Fig. 15. The optimization resut of the second optimization scenario.

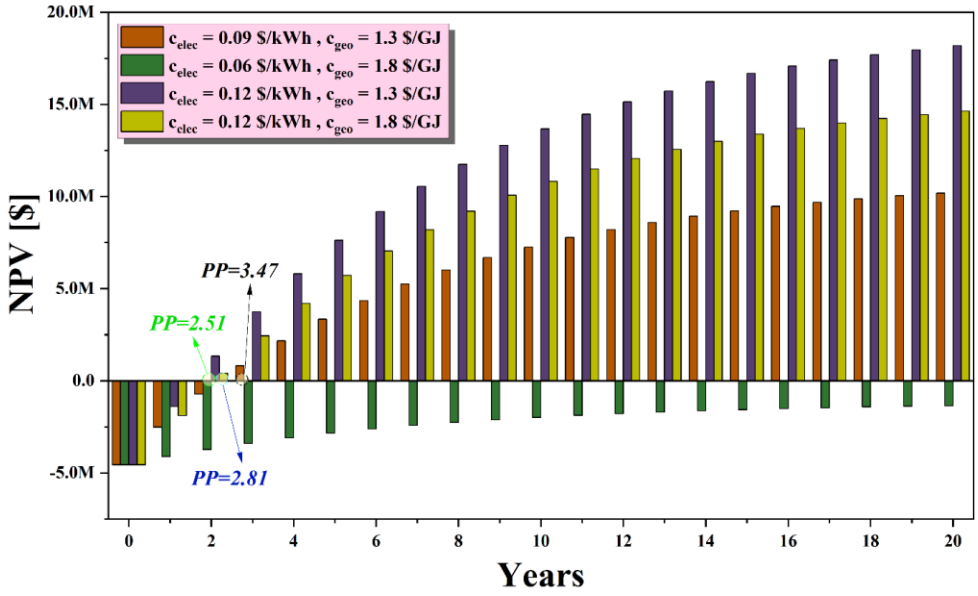

Fig. 16. The NPV diagram for the different prices at the optimum condition.

8. Conclusion

In this paper, a geothermal power system was proposed to generate power. Also, an ORC subsystem with the zeotropic working fluid was employed to recover the geothermal system waste energy and generate more power. Comprehensive mass, energy, exergy, and exergoeconomic analysis were applied to evaluate the proposed system. Then, a parametric study was performed to study the effect of vapor generation, zeotropic mass mixture's mass fraction, and the first and second separator inlet pressure on the main performance criteria of the designed system. The NPV index was evaluated for four different prices scenarios to evaluate the proposed system's exergoeconomic performance. Finally, an

MOPSO approach was employed to obtain the optimum condition of system for two scenarios. All conducted studies led to the following conclusions:

The vapor generator, steam turbine, and the separators are the most exergy destroyer components in the designed system.

Increasing the vapor generator operational temperature decreases the exergy destruction for all zeotropic mixture mass fractions.

The evaporation temperature's rise improves the thermal and exergetic efficiencies. Specially the ORC subsystem exergetic efficiency.

Increasing the first separator inlet pressure reduces the total exergy destruction and improves the energy and exergy efficiencies of the proposed system.

Increasing the second separator inlet pressure increases the exergy destruction and declines the energy and exergy efficiencies of the proposed system.

Increasing the electricity sale price by about 33% decreases the payback period and improves purchased net profit by about 29% and 78.29%, respectively, while increasing the geofluid by about 38.4% increases the payback by about 12.4%, and reducing the purchased net profit by about 19.5%.

Considering the energy efficiency and payback period as the optimization cost function improves the net power production and energy efficiency but increases the payback period slightly.

Considering the exergy efficiency and payback period as the optimization cost function improves the exergy efficiency and payback period of the proposed system.

REFERENCES

[1] S. E. Hosseinizadeh, E. Ghamati, A. Jahangiri, S. Majidi, I. Khazaee, and M. A. F. Aliabadi, "Reduction of water droplets effects in steam turbine blade using Multi-objective optimization of hot steam injection," *International Journal of Thermal Sciences*, vol. 187, p. 108155, 2023.

[2] G. Shu, L. Liu, H. Tian, H. Wei, and G. Yu, "Parametric and working fluid analysis of a dual-loop organic Rankine cycle (DORC) used in engine waste heat recovery," *Appl Energy*, vol. 113, pp. 1188–1198, 2014.

[3] M. A. F. Aliabadi, E. Lakzian, A. Jahangiri, and I. Khazaei, "Numerical investigation of effects polydispersed droplets on the erosion rate and condensation loss in the wet steam flow in the turbine blade cascade," *Appl Therm Eng*, vol. 164, p. 114478, 2020.

[4] A. Habibollahzade, Z. K. Mehrabadi, and C. N. Markides, "Comparative thermoeconomic analyses and multi-objective particle swarm optimization of geothermal combined cooling and power systems," *Energy Convers Manag*, vol. 234, p. 113921, 2021.

[5] F. A. Boyaghchi and P. Heidarnejad, "Thermoeconomic assessment and multi objective optimization of a solar micro CCHP based on Organic Rankine Cycle for domestic application," *Energy Convers Manag*, vol. 97, pp. 224–234, 2015.

[6] J. Song, P. Loo, J. Teo, and C. N. Markides, "Thermo-economic optimization of organic Rankine cycle (ORC) systems for geothermal power generation: A comparative study of system configurations," *Front Energy Res*, vol. 8, p. 6, 2020.

[7] M. Kanoglu and A. Bolatturk, "Performance and parametric investigation of a binary geothermal power plant by exergy," *Renew Energy*, vol. 33, no. 11, pp. 2366–2374, 2008.

[8] S. J. Zarrouk and M. H. Purnanto, "Geothermal steam-water separators: Design overview," *Geothermics*, vol. 53, pp. 236–254, 2015.

[9] M. Yari, "Exergetic analysis of various types of geothermal power plants," *Renew Energy*, vol. 35, no. 1, pp. 112–121, 2010.

[10] M. Zeyghami, "Performance analysis and binary working fluid selection of combined flash-binary geothermal cycle," *Energy*, vol. 88, pp. 765–774, 2015.

[11] A. H. Mosaffa, N. H. Mokarram, and L. G. Farshi, "Thermo-economic analysis of combined different ORCs geothermal power plants and LNG cold energy," *Geothermics*, vol. 65, pp. 113–125, 2017.

[12] C. Luo, L. Huang, Y. Gong, and W. Ma, "Thermodynamic comparison of different types of geothermal power plant systems and case studies in China," *Renew Energy*, vol. 48, pp. 155–160, 2012.

[13] S. M. Bina, S. Jalilinasrabady, and H. Fujii, "Thermo-economic evaluation of various bottoming ORCs for geothermal power plant, determination of optimum cycle for Sabalan power plant exhaust," *Geothermics*, vol. 70, pp. 181–191, 2017.

[14] S. M. Bina, S. Jalilinasrabady, and H. Fujii, "Exergoeconomic analysis and optimization of single and double flash cycles for Sabalan geothermal power plant," *Geothermics*, vol. 72, pp. 74–82, 2018.

[15] M. Abdolalipouradl, F. Mohammadkhani, and S. Khalilarya, "A comparative analysis of novel combined flash-binary cycles for Sabalan geothermal wells: Thermodynamic and exergoeconomic viewpoints," *Energy*, vol. 209, p. 118235, 2020.

[16] Z. Guzović, B. Majcen, and S. Cvetković, "Possibilities of electricity generation in the Republic of Croatia from medium-temperature geothermal sources," *Appl Energy*, vol. 98, pp. 404–414, 2012.

[17] J. Li, Z. Ge, Y. Duan, Z. Yang, and Q. Liu, "Parametric optimization and thermodynamic performance comparison of single-pressure and dual-pressure evaporation organic Rankine cycles," *Appl Energy*, vol. 217, pp. 409–421, 2018.

[18] Z. Ge, J. Li, Q. Liu, Y. Duan, and Z. Yang, "Thermodynamic analysis of dual-loop organic Rankine cycle using zeotropic mixtures for internal combustion engine waste heat recovery," *Energy Convers Manag*, vol. 166, pp. 201–214, 2018.

[19] W. Li, X. Feng, L. J. Yu, and J. Xu, "Effects of

evaporating temperature and internal heat exchanger on organic Rankine cycle," *Appl Therm Eng*, vol. 31, no. 17–18, pp. 4014–4023, 2011.
[20] L. Zhao and J. Bao, "Thermodynamic analysis of organic Rankine cycle using zeotropic mixtures," *Appl Energy*, vol. 130, pp. 748–756, 2014.
[21] J. Wang, J. Wang, Y. Dai, and P. Zhao, "Thermodynamic analysis and optimization of a flash-binary geothermal power generation system," *Geothermics*, vol. 55, pp. 69–77, 2015.
[22] A. Sohani, H. Sayyaadi, and M. Zeraatpisheh, "Optimization strategy by a general approach to enhance improving potential of dew-point evaporative coolers," *Energy Convers Manag*, vol. 188, pp. 177–213, 2019.
[23] T. Parikhani, J. Jannatkhah, A. Shokri, and H. Ghaebi, "Thermodynamic analysis and optimization of a novel power generation system based on modified Kalina and GT-MHR cycles," *Energy Convers Manag*, vol. 196, pp. 418–429, 2019.
[24] H. Rostamzadeh, M. Ebadollahi, H. Ghaebi, and A. Shokri, "Comparative study of two novel micro-CCHP systems based on organic Rankine cycle and Kalina cycle," *Energy Convers Manag*, vol. 183, pp. 210–229, 2019.
[25] N. Mahdavi, H. Ghaebi, and A. Minaei, "Proposal and multi-aspect assessment of a novel solar-based trigeneration system; investigation of zeotropic mixture's utilization," *Appl Therm Eng*, vol. 206, p. 118110, 2022.
[26] S. Ahmadi, H. Ghaebi, and A. Shokri, "A comprehensive thermodynamic analysis of a novel CHP system based on SOFC and APC cycles," *Energy*, vol. 186, p. 115899, 2019.
[27] F. Hamrang, S. M. S. Mahmoudi, and M. A. Rosen, "A novel electricity and freshwater production system: performance analysis from reliability and exergoeconomic viewpoints with multi-objective optimization," *Sustainability*, vol. 13, no. 11, p. 6448, 2021.
[28] F. Hamrang, A. Shokri, S. M. S. Mahmoudi, B. Ehghaghi, and M. A. Rosen, "Performance analysis of a new electricity and freshwater production system based on an integrated gasification combined cycle and multi-effect desalination," *Sustainability*, vol. 12, no. 19, p. 7996, 2020.
[29] S. Eshaghi and F. Hamrang, "An innovative techno-economic analysis for the selection of an integrated ejector system in the flare gas recovery of a refinery plant," *Energy*, vol. 228, p. 120594, 2021.
[30] Y. A. Cengel, M. A. Boles, and M. Kanoğlu, *Thermodynamics: an engineering approach*, vol. 5. McGraw-hill New York, 2011.
[31] P. Ding *et al.*, "Multi-objective optimization and exergoeconomic analysis of geothermal-based electricity and cooling system using zeotropic mixtures as the working fluid," *J Clean Prod*, vol. 294, p. 126237, 2021.